Clim Dyn
DOI 10.1007/s00382-015-2530-4

The de-correlation of westerly winds and westerly-wind stress over the Southern Ocean during the Last Glacial Maximum

Wei Liu · Jian Lu · L. Ruby Leung · Shang-Ping Xie · Zhengyu Liu · Jiang Zhu

Received: 6 October 2014 / Accepted: 13 February 2015

Abstract Motivated by indications from paleo-evidence, this paper investigates the changes of the Southern Westerly Winds (SWW) and westerly-wind stress between the Last Glacial Maximum (LGM) and pre-industrial in the PMIP3/CMIP5 simulations, highlighting the role of Antarctic sea ice in modulating the wind effect on ocean. Particularly, a de-correlation occurs between the changes in SWW and westerly-wind stress, caused primarily by an equatorward expansion of winter Antarctic sea ice that undermines the efficacy of wind in generating stress over the liquid ocean. Such de-correlation may reflect the LGM condition in reality, in view of the fact that the model which simulates this condition has most fidelity in simulating modern SWW and Antarctic sea ice. Therein two models stand out for their agreements with paleo-evidence regarding the change of SWW and the westerly-wind stress. They simulate strengthened and poleward-migrated LGM SWW in the atmosphere, consistent with the indications from dust records. Whilst in the ocean, they well capture an equatorward-shifted pattern of the observed oceanic front shift, with most pronounced equatorward-shifted westerly wind stress during the LGM.

Keywords Southern Westerly Winds · Westerly wind stress · Antarctic sea ice · LGM · PMIP3/CMIP5

W. Liu (✉) · S.-P. Xie
CASPO, Scripps Institution of Oceanography, University of California, San Diego, 9500 Gilman Drive, La Jolla, CA 92093, USA
e-mail: wel109@ucsd.edu

W. Liu · J. Lu · L. R. Leung
Pacific Northwest National Laboratory, Richland, WA, USA

Z. Liu · J. Zhu
Department of Atmospheric and Oceanic Sciences, Nelson Center for Climatic Research, University of Wisconsin-Madison, Madison, WI, USA

Z. Liu
LaCOAS, School of Physics, Peking University, Beijing, China

1 Introduction

The Southern Westerly Winds (SWW) are generally considered as one of vital factors responsible for the glacial to interglacial CO_2 increase observed in ice-cores at each glacial termination (e.g., Menviel et al. 2008; Anderson et al. 2009; Siani et al. 2013). In a so-called "westerly shift" hypothesis (Toggweiler et al. 2006), a poleward-shifted or stronger westerly is expected to enhance the Southern Ocean (SO) upwelling, amplify the deep-ocean ventilation and allow more respired CO_2 outgassing into the atmosphere during the deglaciation, and vice versa. Albeit seeming plausible, this hypothesis is hampered by great uncertainties in the meridional shift of SWW from the Last Glacial Maximum (LGM) to modern climate. Indications from paleo-proxy evidences are equivocal with regard to the displacement and strength change of SWW during the LGM (Kohfeld et al. 2013). They highly depend on which perspective and which category of paleo-data are selected for examination (Kohfeld et al. 2013).

From an atmospheric perspective, indications seem contradictory from terrestrial moisture records but appear generally consistent from dust records. The latter favors a strengthened and poleward-shifted westerly during the LGM. To be more specific, terrestrial moisture (e.g., pollen and lake level) proxies suggest either a poleward or an equatorward displacement of the LGM SWW from their present position. In one end, pollen from marine sediments

Published online: 22 February 2015

off Chile coast (37°–41°S, 73.36°–74.45°W) depicts prominent hyper-humid vegetation (North Patagonian and Subantarctic forests and parkland) during the LGM, implying a sustained equatorward migration of SWW (Heusser et al. 2006a, b). In the other end, pollen and lake level records from Central and South America (33°–41°S, 66°–71°W) and Australia (33°S, 158.1°E) indicate a far drier LGM condition and therefore a poleward shift of the westerly circulation (Markgraf 1989; Williams et al. 2006). These contradictory results cast doubt on the usage of moisture proxies as an observational evidence (Sime et al. 2013), especially considering the fact that most moisture proxies are confined within land (c.f., Kohfeld et al. 2013), a small portion of area swept by SWW. By contrast, dust deposition data are more representative in space. They can be obtained from ice cores, marine sediments, and terrestrial (loess) deposits and thus cover both land and ocean (e.g., Kohfeld and Harrison 2001; Mahowald et al. 2006). Most dust records show a much larger dust deposition rate during the LGM compared to late Holocene (e.g., Petit et al. 1999; Delmonte et al. 2002; Wolff et al. 2006), which consistently suggests a strengthened and poleward-shifted westerly during the LGM.

From an oceanic perspective, paleo-evidence uniformly supports an equatorward shift of SWW. For example, based on isotopes and planktonic foramaniferal assemblages, reconstructed temperatures indicate a northward migration of oceanic front system (Subtropical Front (STF), Polar Front (PF) and Subantarctic Front (SAF)) and thus an equatorward shift of SWW during the LGM (e.g., Prell et al. 1980; Nelson et al. 2000; Gersonde et al. 2003, 2005). Another example comes from "Agulhas leakage," a circulation of warm salty surface waters into the South Atlantic Ocean. Based on "Agulhas Leakage Fauna" (Peeters et al. 2004), Agulhas leakage appears reduced during the LGM, implying equatorward shifts in the STF and westerly winds (Bard and Rickaby 2009). Thereby, questions arise naturally, i.e., what is indeed the SWW shift during the LGM? Or more provokingly, why does the westerly shift appear so different between the atmospheric and oceanic perspectives? These questions cannot be simply answered by digging into existing paleo-data archive; a model-proxy data comparison may shed lights on the answer. Using physically based models that represent both atmosphere and ocean, the latter approach may help synthesize the atmospheric and oceanic perspectives and enable an assessment of the LGM westerly shift from a dynamic framework.

Nevertheless, one issue should be raised before an employment of model-proxy data comparison. We find that many paleo-modeling studies in history were used to examining the changes of SWW between the LGM and modern climates from an atmospheric perspective (e.g., Valdes 2000; Wyrwoll et al. 2000; Kitoh et al. 2001; Chavaillaz et al. 2013; Rojas 2013). The lower-level westerly (850 hPa zonal winds) was usually selected for analyses, since it is crucial for moisture transport and indicative of westerly-related storm track, with effects from the boundary layer avoided as well. This choice looks reasonable for atmosphere, but may not be for ocean, especially considering the wind-driven upwelling in the loop of the "westerly shift" hypothesis. More specifically, the low level wind is not equivalent to the momentum forcing of ocean, because: (1) the low-level westerly could be substantially modulated by boundary layer effects before its impact reaches the surface (Sime et al. 2013); (2) it is the sea surface wind stress instead of the near-surface winds that controls the oceanic fronts and drives the SO upwelling (e.g., Shin et al. 2003; Kim et al. 2003; Otto-Bliesner et al. 2006; Rojas et al. 2009; Brady et al. 2013). Large differences may exist between the two. Hence a careful examination on the relationship among the low-level SWW, near surface westerly and westerly-wind stress is in order.

In this paper, we focus on eight models participating in the latest Paleoclimate Modelling Intercomparison Project phase 3 (PMIP3)/Coupled Model Intercomparison Project phase 5 (CMIP5) and analyze SWW and westerly wind stress between the LGM and modern climates. The rest of the paper is structured as follows. Section 2 provides the information of the PMIP3/CMIP5 simulations, paleo- and present observational data included in the study and approaches for analyses. In Sect. 3, we conduct inter-model and model-proxy data comparisons with regard to SWW and wind stress between the LGM and modern climates, and find that Antarctic sea ice is the key to reconciling the perspectives from the atmosphere and ocean. In particular, the LGM Antarctic sea ice can cause a de-correlation between the westerly wind shift in the atmosphere (poleward) and wind stress shift over the liquid ocean (equatorward), consistent with the indications from paleo-data evidences. Concluding remarks and further discussions are given in Sect. 4.

2 Data and approach

To compare between the glacial and modern climates, both model and observational data are used. For models, two types of experiments from PMIP3/CMIP5 have been analyzed: the LGM and pre-industrial (PI) simulations from eight models: CCSM4, CNRM-CM5, FGOALS-g2, GISS-E2-R, IPSL-CM5A-LR, MIROC-ESM, MPI-ESM-P and MRI-CGCM3 (Braconnot et al. 2012; Taylor et al. 2012, c.f. Table 1). Variables analyzed include low-level winds (on pressure coordinate), near surface (10 m) winds, surface wind stress exerted on the liquid ocean. Note that the sea surface wind stress here refers to the stress driving the

Table 1 The PMIP3/CMIP5 models used in this study and their development groups, model abbreviations, and atmosphere and ocean components the LGM and PI simulations

Modeling group	Model abbreviation	Atmosphere component	Ocean component
National Center for Atmospheric Research, USA	CCSM4	26 vertical layers 1.25° × 1°	60 vertical layers 1.11° × (0.27°–0.54°)
Center National de Recherches météorologiques (CNRM), France	CNRM-CM5	31 vertical layers 1.4° × 1.4°	42 vertical layers 1° × (0.33°–1°)
State Key Laboratory of Numerical Modeling for Atmospheric Sciences and Geophysical Fluid Dynamics, China	FGOALS-g2	26 vertical layers 2.8° × 1.6°	30 vertical layers ~1° × 1°
National Aeronautics and Spatial Administration, Goddard Institute for Spatial Studies, USA	GISS-E2-R	40 vertical layers 2.5° × 2°	32 vertical layers 1° × 1.25°
Institut Pierre Simon Laplace, France	IPSL-CM5A-LR	39 vertical layers 3.75° × 1.8°	31 vertical layers ~2° × 2°
Japan Agency for Marine-Earth Science and Technology, Atmosphere and Ocean Research Institute, the University of Tokyo and National Institute for Environmental Studies, Japan	MIROC-ESM	80 vertical layers 2.8° × 2.8°	44 vertical layers ~1.4° × 1°
Max Planck Institute for Meteorology, Germany	MPI-ESM-P	47 vertical layers ~1.9° × 1.9°	40 vertical layers ~1.5° × 1.5°
Meteorological Research Institute, Japan	MRI-CGCM3	48 vertical layers 1.1° × 1.1°	51 vertical layers 1° × 0.5°

Table 2 SWW and westerly-wind stress in the PMIP3/CMIP5 models, as well as their changes between two climates (LGM minus PI)

Model	u_s	τ_x	$\Delta\phi(u_{max850})$ (degrees)	$\Delta\phi(u_{smax})$ (degrees)	$\Delta\phi(\tau_{xmax})$ (degrees)
CCSM4	n/a	a	−0.245	n/a	1.573
CNRM-CM5	a	a	1.473	0.951	1.112
FGOAL-g2	n/a	n/a	−1.642	n/a	n/a
GISS-E2-R	a	n/a	1.704	1.350	n/a
IPSL-CM5A-LR	a	a	1.290	0.941	1.176
MIROC-ESM	a	a	−0.704	−1.007	−0.051
MPI-ESM-P	a	a	−0.405	−0.124	0.064
MRI-CGCM3	a	a	−3.697	−5.021	1.489

Us, τ_x denotes near surface zonal winds and zonal wind stress, respectively, which are available (denoted as "a") from five models and apparently unavailable (denoted as "n/a") from the other three models. $\Delta\phi(u_{max850})$, $\Delta\phi(u_{smax})$ and $\Delta\phi(\tau_{xmax})$ are the latitudinal changes of 850 hPa zonal wind maximum, near surface zonal wind maximum and zonal wind stress maximum (LGM minus PI), respectively, in unit of degrees

liquid ocean (Yang 2006), including the open ocean and the ocean water under the cover of sea ice. As shown in Table 2, the near surface wind and sea surface wind stress are not available in some models. For observations, several sets of reanalysis and reconstruction data are employed. Under the modern climate, low-level winds, near surface winds and sea-ice extent are extracted from the NCAR/NCEP reanalysis dataset (Kalney et al. 1996). Sea surface wind stress is obtained from an updated product of Scatterometer Climatology of Ocean Winds (SCOW; Risien and Chelton 2008) and mostly limited to the open ocean. Under the LGM climate, only sea-ice extent is available, which is from a LGM reconstruction (Schäfer-Neth and Paul 2003; SP03 thereafter).

For both models and observations, only the climatological mean of the variables in interest are examined. The model climatology is calculated as a 100-year average. The climatology for the observations is estimated as the average over the time period when the data is available. The position and strength of the cores of SWW and westerly-wind stress are determined by first taking a zonal mean of the zonal winds (wind stress) and then employing a quadratic interpolation around the grid point of maximum winds (wind stress) (c.f., Chavaillaz et al. 2013).

For the purpose of evaluating the PMIP3/CMIP5 model simulations of the austral winter (JJA) Antarctic sea-ice cover during the LGM, we adopt the LGM sea-ice reconstruction by SP03 as the observation benchmark. Since current sea-ice reconstructions on geological timescales rely on indirect observations obtained from scattered marine and ice core records, it is hard to get gridded values of sea-ice concentration. Thereby, reconstructions usually provide

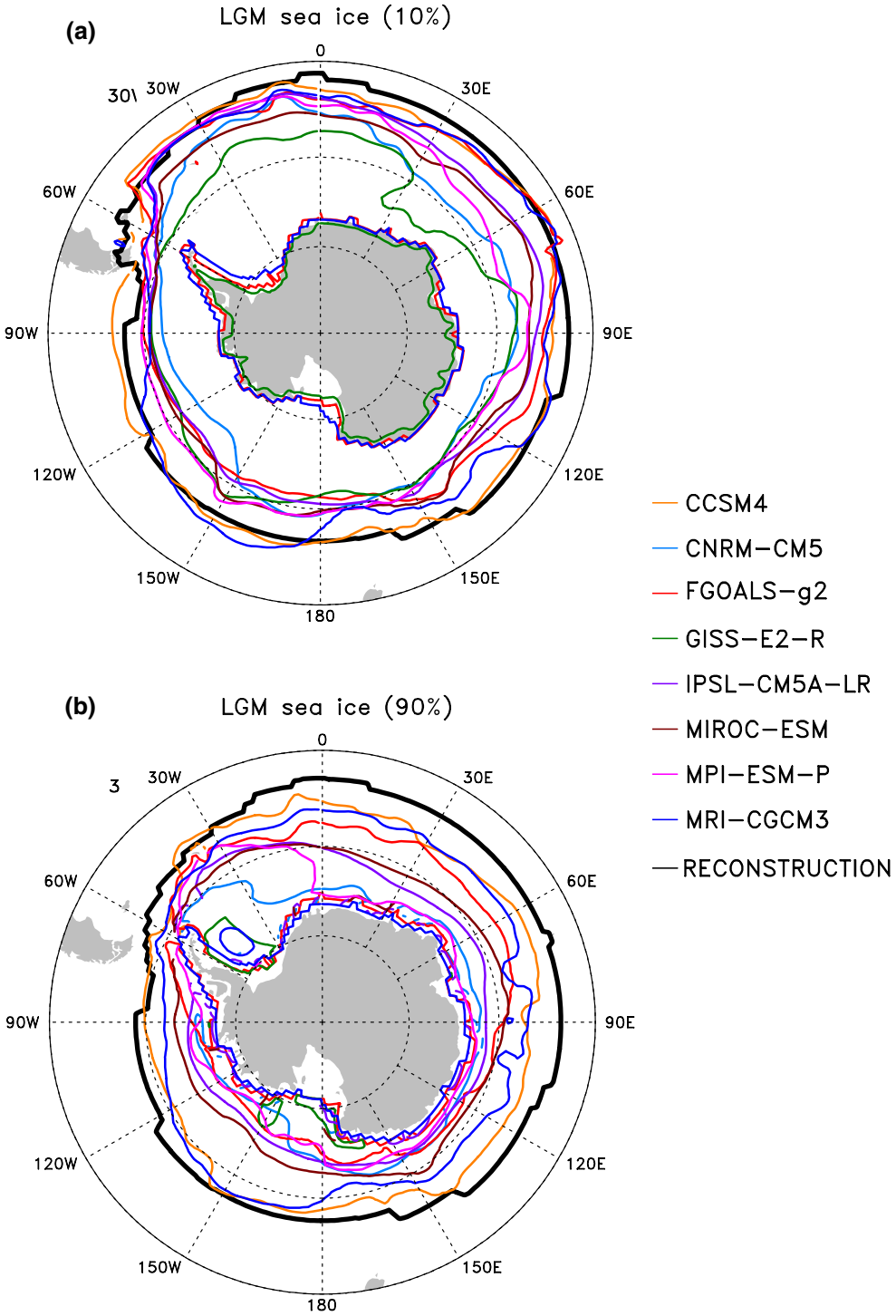

Fig. 1 **a** The 10 % concentration of the SH winter (JJA) sea ice during the LGM from eight PMIP3/CMIP5 models and a paleo-reconstruction by Schäfer-Neth and Paul (2003), which suggests sea-ice presence in general. **b** The same as **a** but for the 90 % concentration, which generally indicates a full-cover of Antarctic sea ice

the estimate of sea-ice presence, such as in SP03. Nevertheless we are still able to employ the winter time sea-ice presence as the proxy for full sea-ice cover (>90 %), considering that the sea-ice concentration drops very rapidly from full-coverage to zero at the edge of sea ice during austral winter.

Figure 1 displays a data-model comparison of the Southern Hemisphere (SH) winter Antarctic sea ice during the

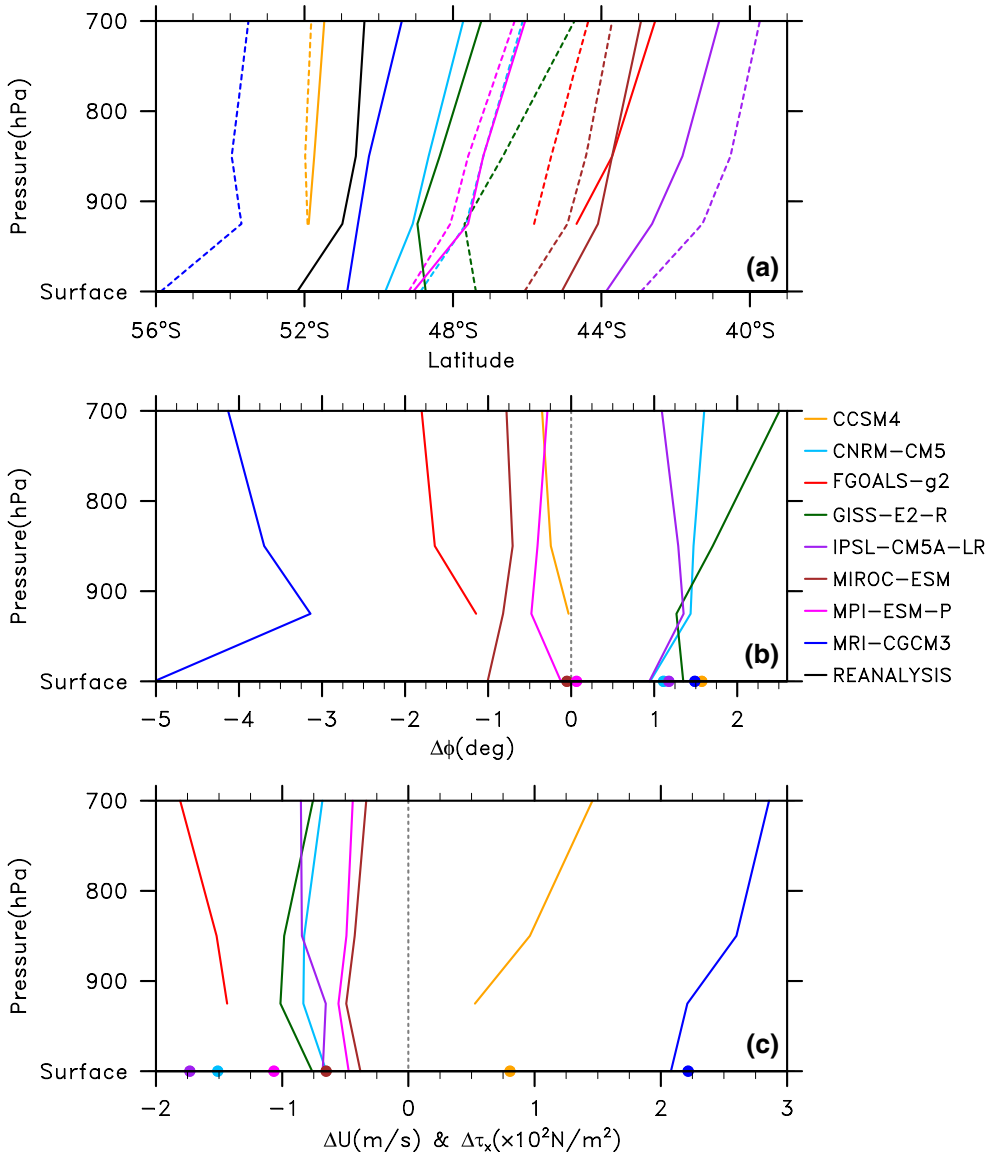

Fig. 2 **a** Locations of SWW (the zonal wind maximum in the SH), from 700 hPa to 925hpa and down to the surface level (10 m) during the LGM (*solid line*) and PI (*dashed line*) from eight PMIP3/CMIP5 models. For PI, result from the NCAR/NCEP reanalysis is used (*black dashed line*). **b** The latitudinal shift of SWW and westerly-wind stress (denoted as *dots at the surface*) between two climates (LGM minus PI). **c** The same as **b** but for the strength change (LGM minus PI). Note here near the surface winds and wind stress are unavailable for several models

LGM, in two contour maps. Panel (a) is the contour map of 10 % sea-ice cover, denoting the edge of the area of sea-ice presence. One can see that CCSM4 and MRI-CGCM3 both reproduce reasonably the LGM sea-ice extent compared to the reconstruction, whereas the other models tend to substantially underestimate the sea-ice extent. Panel (b) is the contour map of 90 % sea-ice cover. Two models, CCSM4 and MRI-CGCM3 have the best agreement with reconstruction, at least for wintertime (Figs. 3i, k, 5a in the later discussion). This assertion is corroborated by an independent comparison analysis by Rojas (2013) between the same group of climate models and another LGM sea-ice reconstruction (Gersonde et al. 2005; Fraser et al. 2009). As a result, some confidence may be assigned to the fidelity of CCSM4 and MRI-CGCM3 in simulating the LGM sea-ice extent and concentration.

3 Results

First, we examine SWW during the LGM and PI in the PMIP3/CMIP5 simulations. Figure 2 shows the LGM/PI

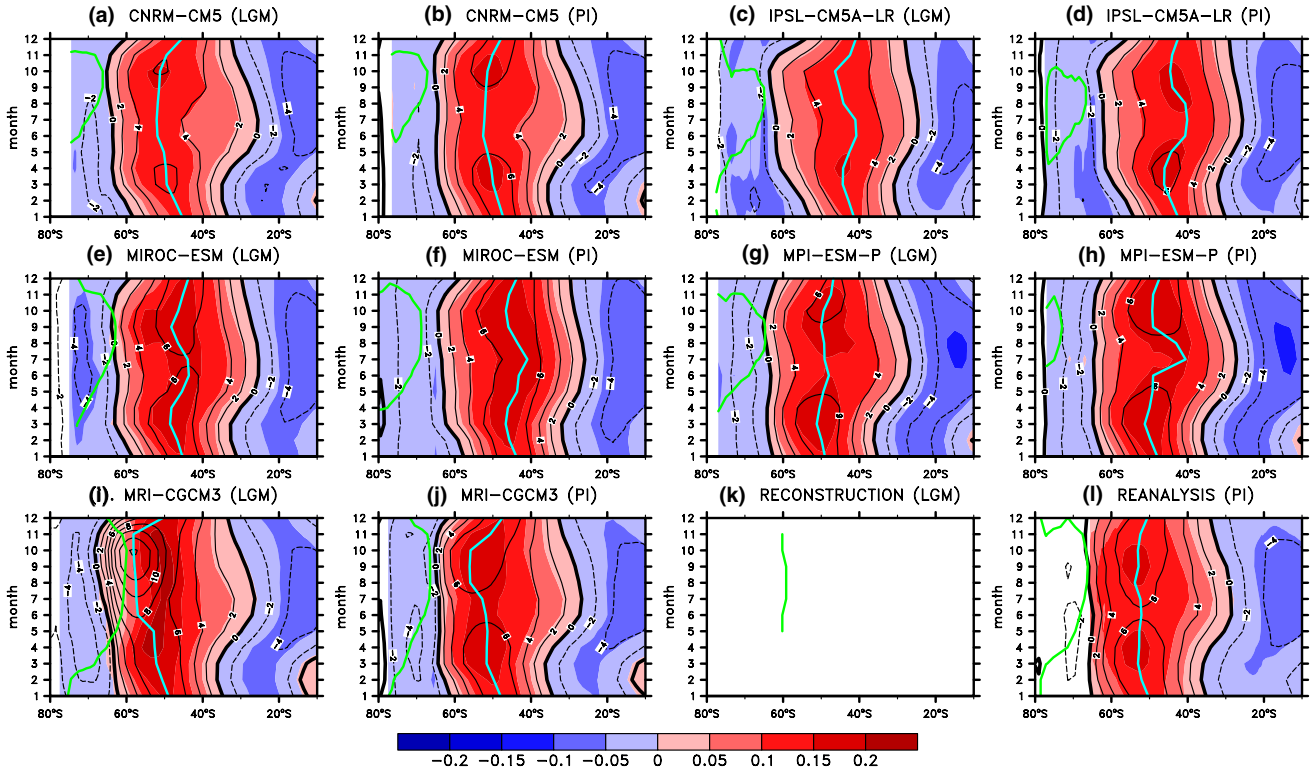

Fig. 3 **a–j** The time–latitude diagram of zonal mean variables: near surface zonal winds (*contour in black*, in unit of m/s), zonal wind stress (*shading* in unit of N/m^2) and 90 % concentration of Antarctic sea ice cover (*green*) during the LGM and PI from five PMIP3/CMIP5 models that have output of all the variables (Table 1). Latitudes of the maximum wind are denoted in *cyan*. **k–l** are the same as **a–j** but for observation. For PI, near surface zonal winds and the sea-ice cover are from the NCAR/NCEP reanalysis and zonal wind stress is from the SCOW product. For the LGM, only sea-ice extent is available, which is from a LGM reconstruction dataset (Schäfer-Neth and Paul 2003)

changes in the latitude and strength of the SWW maximum. Compared to PI, the low-level (above 850 hPa) SWW during the LGM become poleward-shifted and stronger in CCSM4 and MRI-CGCM3, poleward-shifted and weaker in FGOAL-g2, MIROC-ESM, MPI-ESM-P, and equatorward-shifted and weaker in CNRM-CM5, GISS-E2-R and IPSL-CM5A-LR. These different model behaviors were also described in two previous studies on the PMIP3/CMIP5 models (Chavaillaz et al. 2013; Rojas 2013). Apparently, the model results are similar to the moisture proxies, with ambiguous indications of the SWW shift and strength change from the atmospheric perspective. But note that the poleward-shifted and stronger westerly winds simulated in CCSM4 and MRI-CGCM3 are consistent with indication from dust records. Below 850 hPa, winds are modulated by the boundary layer effect that varies with height and behaves differently under the LGM and PI climates. As a result, the westerly shift can be either amplified or undermined in the layer below 850 hPa. Nevertheless, all the models show consistent change between 850 hPa and near surface winds, in both strength (Fig. 2c; Table 2) and position (Fig. 2b; Table 2).

Surprisingly, the change in westerly-wind stress does not always follow the shift of the 850 hPa SWW or even the near surface westerly (Fig. 2b). Despite the fact that the SWW can shift both poleward and equatorward, the surface wind stress almost invariably displaces equatorward in all models, except MIROC-ESM, which shows a very weak poleward shift. In other words, the model results are consistent with indication from marine paleo-evidence and meanwhile, indicate a similar discrepancy to paleo-observation between the atmospheric and oceanic perspectives on the shift of SWW. This further implies that using the SWW shift to infer marine alterations (such as the oceanic front position, Agulhas leakage, etc.) from some proxies (e.g., Kohfeld et al. 2013) can be misleading. Herein the discrepancy is epitomized by the result of MRI-CGCM3, in which the LGM westerly has a poleward shift of 5° at the 10 m level whilst the zonal wind stress exhibits an equatorward shift of 1.5° at the sea surface. The de-correlation between the shifts of winds and wind stress challenges the viability of using SWW to represent the wind stress forcing that the underlying ocean actually sees.

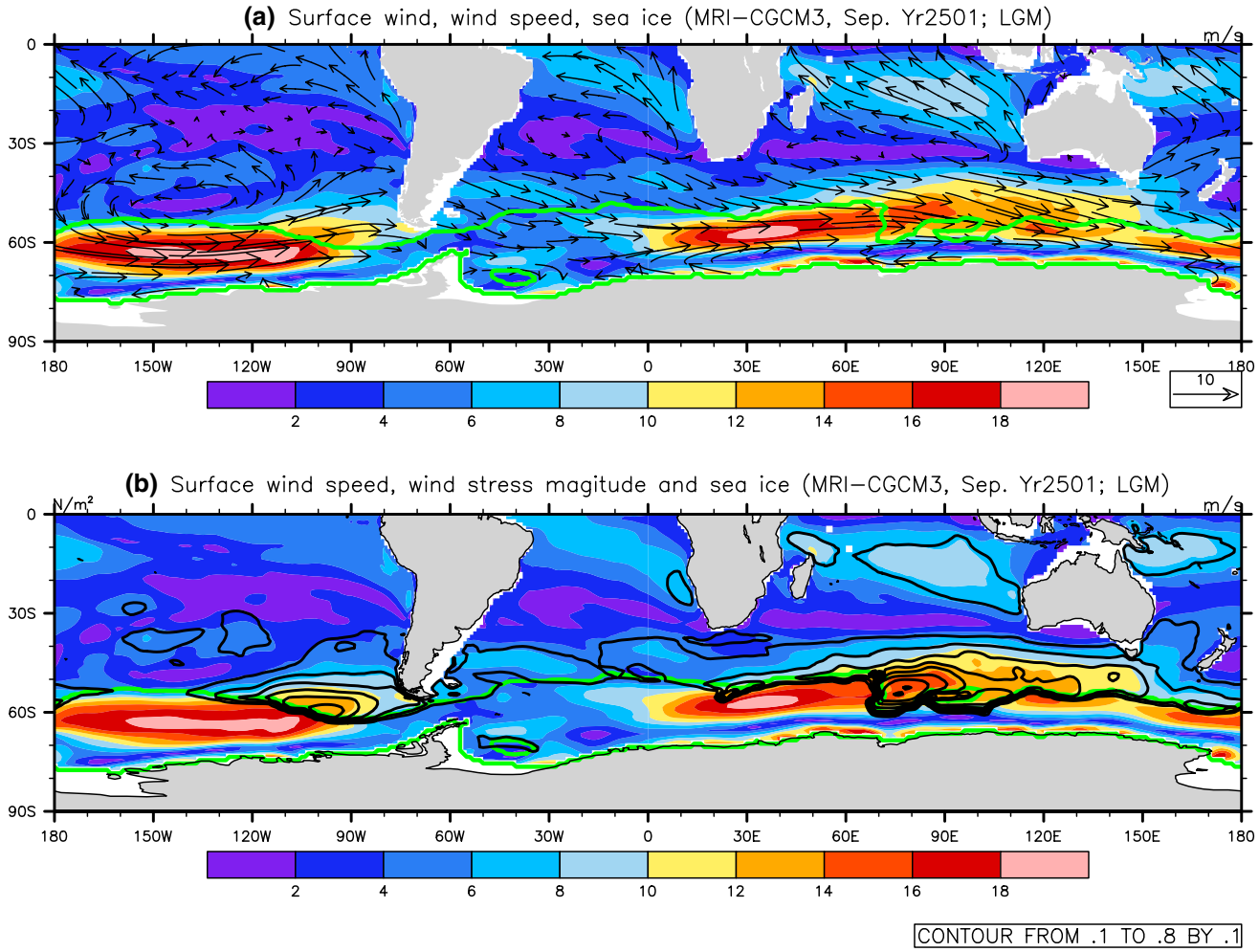

Fig. 4 **a** Surface (10 m) winds (*vector*) and wind speed (*shading* in unit of m/s); **b** wind stress exerted on liquid ocean (*contour* in unit of N/m^2) and wind speed (*shading* in unit of m/s) in September from one arbitrary year (model year 2501) from the MRI-CGCM3 LGM simulation. Contours of 90 % sea-ice concentration are superposed in *green*

The reason for the above de-correlation lies in Antarctic sea ice, which is much more expansive during the LGM than present day or PI. Figure 3 shows the seasonal evolution of the near surface westerly, westerly-wind stress and 90 % sea-ice extent from five climate models. At the LGM, the surface westerly in MRI-CGCM3 exhibits a significant poleward displacement in the SH winter, with its maximum coinciding with the sea-ice edge (~60°S) from June to November (Fig. 3i), as a result of the intricate interplay among surface temperature gradients, sea-ice extent, and the latitude of maximum SWW (Rojas 2013). However, the evolution of wind stress does not follow that of wind. During June-November, the maximum westerly-wind stress even shifts slightly equatorward. This is because much of the strong westerly in winter blows over ice-covered surface where the wind stress drag coefficient is small due to weak turbulent fluxes and very stable stratification of the air layer above (Sime et al. 2013). Then the efficacy of wind in generating stress over the liquid ocean is greatly reduced. As an example, Fig. 4a illustrates the surface wind vector, wind speed and sea ice in September of an arbitrary year (model year 2501) from the MRI-CGCM3 LGM simulation. The westerly with maximum wind speed blows over Antarctic sea ice in two regions: 180°–100°W and 0°–90°E. Due to a substantial reduction of drag coefficient over sea ice in these two regions, the wind stress becomes much smaller there than the surrounding ice-free areas (Fig. 4b). It is also worth noting that this de-correlation only happens in MRI-CGCM3 during the LGM, the only model in the five (note here assessments are limited to the five PMIP3/CMIP5 models that have output all variables needed: near surface zonal winds, zonal wind stress and sea-ice cover) and the only climate period showing large sea-ice expanse reaching as far as 60°S (Fig. 3i). Albeit seemingly anomalous, there are compelling physical reasons behind this exception, making it a plausible scenario for the LGM.

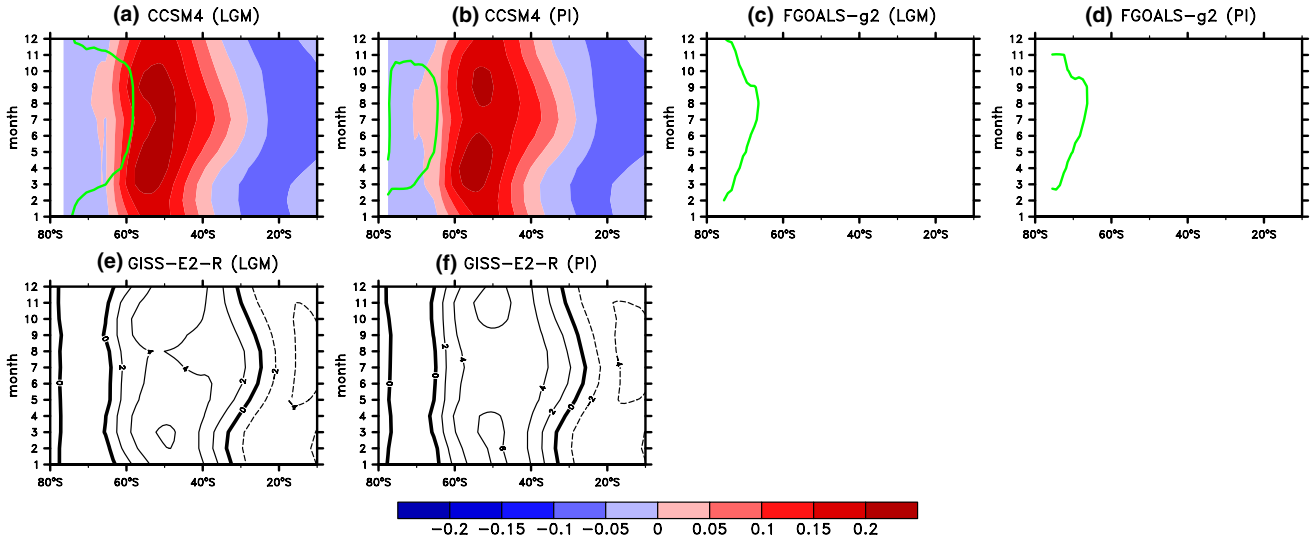

Fig. 5 **a–f** The time–latitude diagram of zonal mean variables: near surface zonal winds (*contour* in *black*, in unit of m/s), zonal wind stress (*shading* in unit of N/m^2) and 90 % concentration of Antarctic sea ice cover (*green*) during the LGM and PI from three PMIP3/CMIP5 models which do not have output of all variables (Table 2). Contours of 90 % sea-ice cover are visually lack in plots **e** and **f** since the zonal mean concentration of Antarctic sea ice in the GISS-E2-R model is below 90 % in both LGM and PI climates

In fact, MRI-CGCM3 is arguably the model with the least bias in simulating SWW, westerly-wind stress and sea ice amongst the PMIP3/CMIP5 models. SWW in MRI-CGCM3 resemble the observation, both in vertical profile (Fig. 2a) and in seasonality (Fig. 3); its jet position is the closest to the NCAR/NCEP reanalysis. In addition, the seasonal variations and meridional extent of Antarctic sea ice in MRI-CGCM3 are the closest to those in observations, for both PI and LGM climates (Figs. 1, 3). Particularly, under PI climate, MRI-CGCM3 simulates surface westerly that approaches the edge of the Antarctic sea ice in winter, around 65°S, an observed feature that has yet to be replicated by other models. As Antarctic sea ice advances equatorward during the LGM, the southern portion of the surface westerly sweeps over the surface of sea ice and hence a de-correlation between SWW and westerly-wind stress ensues. Similar de-correlation between the shifts of low-level westerly and westerly-wind stress has also been found in CCSM4 (Fig. 2b; Table 2), another model with good fidelity in simulating the location of the SH jet (Fig. 2a) and Antarctic sea ice (Figs. 1, 5).

A further support for the plausibility in the simulations of MRI-CGCM3 and CCSM4 comes from the perspective of oceanic front shifts. In comparison to the modern sea surface temperature (SST), paleo-proxy reconstruction by SP03 illustrates a strong cooling between the latitude band 40°–50°S in the modern Sub-Antarctic Zone (SAZ), a relatively weaker cooling both north of the modern STF and south of the modern PF zone (Fig. 6h), suggesting an equatorward displacement of oceanic front system over the SO in general [this feature is also confirmed in several other paleo-reconstructions (e.g., Waelbroeck et al. 2009; Kohfeld et al. 2013)]. Customarily, such equatorward displacement of oceanic fronts is considered to be a marine evidence for the equatorward shift of SWW and the westerly-wind stress. In PMIP3/CMIP5, albeit most models simulate an equatorward shift of the wind stress (Table 2), only MRI-CGCM3 (Fig. 6g) and CCSM4 (Fig. 6a) capture the pattern of the observed oceanic front shifts. All the evidences point to the greater probability of the LGM scenarios simulated by these two models.

4 Conclusion and discussion

In this study, the SWW shift during the LGM has been investigated among the PMIP3/CMIP5 simulations, with a focus on the changes in SWW, westerly-wind stress and Antarctic sea ice from the LGM to PI. At 850 hPa, six models simulate weaker or equatorward-shifted SWW during the LGM, whilst the other two, CCSM4 and MRI-CGCM3, simulate stronger and poleward-shifted SWW. A de-correlation has been found in MRI-CGCM3 and CCSM4 between the changes in SWW and westerly-wind stress. This de-correlation can be attributed to the expansive Antarctic sea ice during the LGM, which reduces the wind stress by compromising the drag coefficient. Herein we argue that such de-correlation could happen in reality during the glacial period in view of the fact that the two models simulate the distributions of SWW and Antarctic sea ice with greater fidelity under modern climate. Indeed, the plausibility of the LGM scenarios by MRI-CGCM3 and

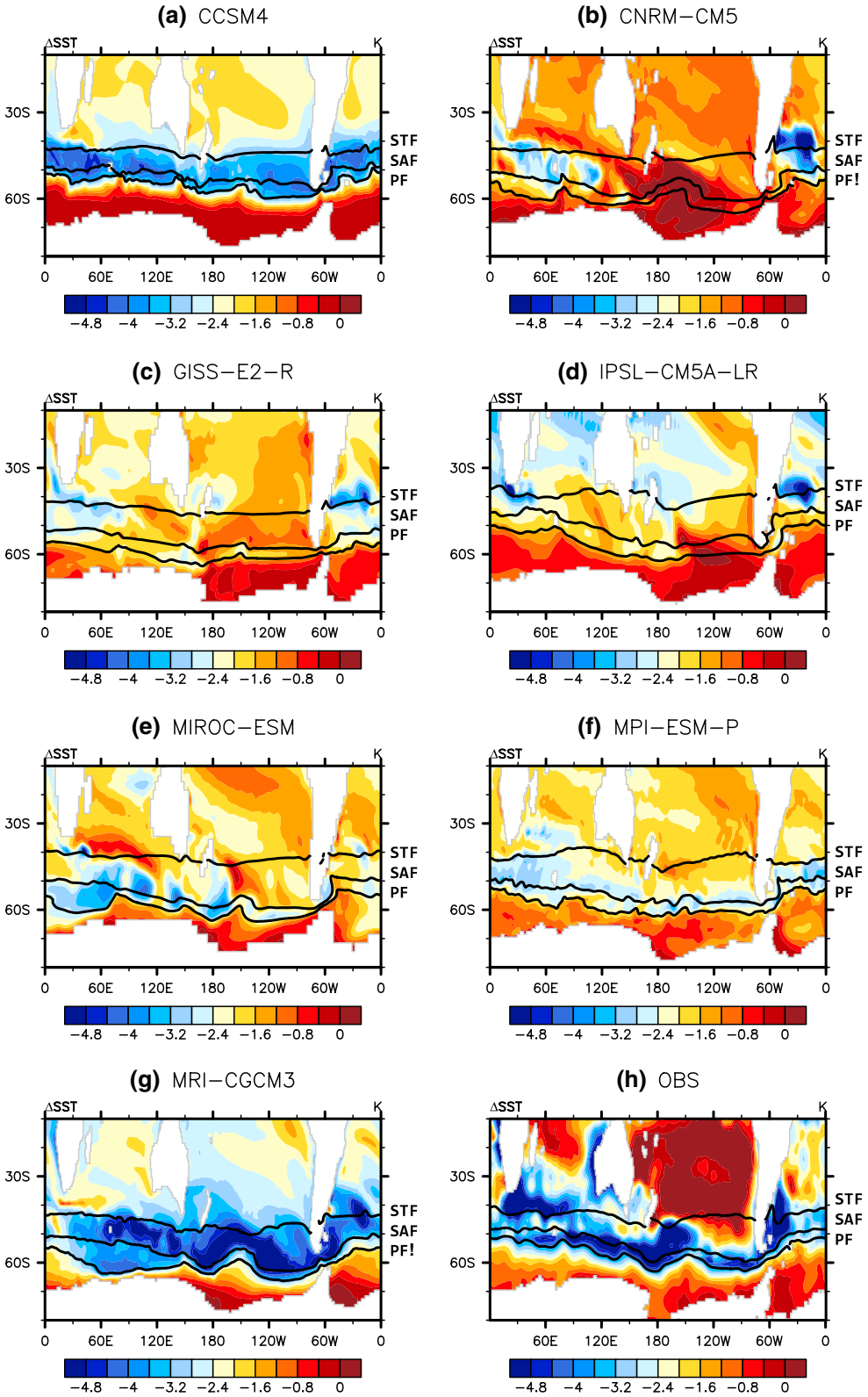

Fig. 6 Changes in the SST (*shading* in unit of K) during the LGM relative to PI from **a**–**g** seven PMIP3/CMIP5 models and **h** observation. The observational LGM SST is from a paleo-reconstruction by Schäfer-Neth and Paul (2003) and the modern SST is from World Ocean Atlas (WOA) 1998. In all panels, *black lines* represent position of the major modern-day oceanic fronts: the Subtropical Front (STF), Polar Front (PF) and Subantarctic Front (SAF), following the definition in Orsi et al. (1995)

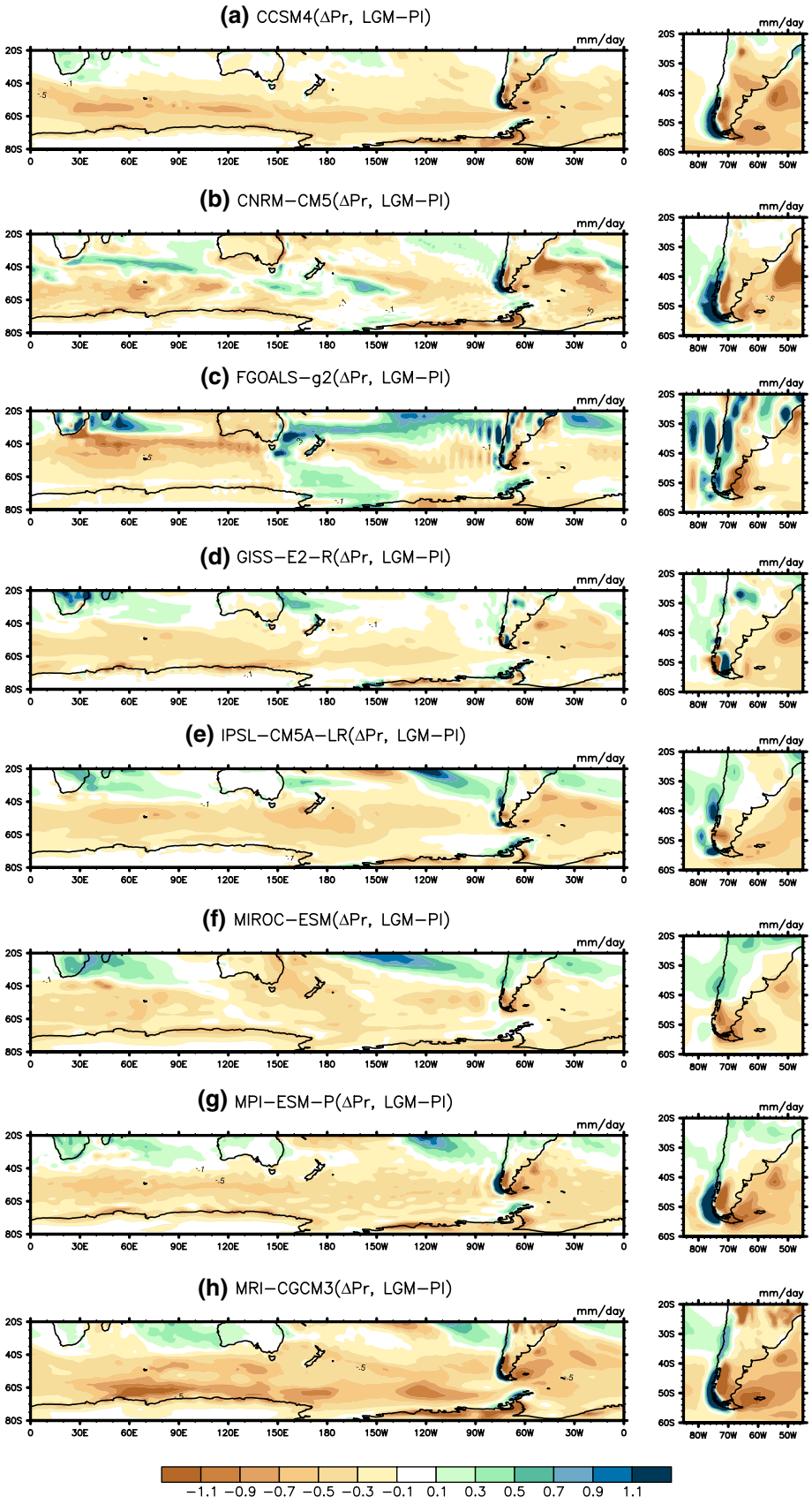

Fig. 7 (*Left panel*, **a**–**h**) changes in annual precipitation (*shading* in unit of mm/day) during the LGM relative to PI from eight PMIP3/CMIP5 models. (*Right panel*) a zoom in view of the Southern South America, featuring with precipitation change in the Southern Andres mountains and Patagonia region

CCSM4 is supported in two ways. From an atmospheric perspective, both models simulate a strengthened and poleward-migrated westerly during the LGM, as consistent with the indication from dust records. From an oceanic perspective, they are ranked the best models in capturing the equatorward-shifted pattern of the observed oceanic front shifts, with most pronounced equatorward-shifted westerly wind stress during the LGM.

In addition, we would like to point out that the model results could facilitate the interpretation of the puzzling moisture-proxy evidence. As described in Sect. 1, great spatial variations emerge in the moisture-indicated SWW shifts over the southern South America. Proxies indicate enhanced precipitation and thus an equatorward westerly shift off Chile coast (32.8°–41°S, 72°–74.45°W) but reduced precipitation and a poleward westerly displacement on the Argentina side (33°–41°S, 66°–71°W). It is hard to imagine how much the precipitation varies within such a small region while the model results seem to give the answer. Figure 7 illustrates the change of LGM precipitation relative to PI among eight PMIP3/CMIP5 models. Except GISS-E2-R and MIROC-ESM, most models consistently simulate an east–west dipole of precipitation anomalies in the southern tip of South America (the Patagonia area), with more precipitation on the Chilean side and neighboring sea and less precipitation on the Argentina side. This feature is more related to a local orographic effect rather than the migration of westerly-related storm track, or alterations in global hydrological cycle (e.g., Held and Soden 2006; Boos 2012). From previous literatures (c.f. Paruelo et al. 1998 for a review), rainfall pattern in this area is dominated by the Andes Mountains, whose north–south distribution imposes a barrier for humid Pacific air masses along the storm track. Owing to an orographic effect, most of the moisture in the maritime air masses precipitates on the Chilean side, and the air becomes hotter and drier through adiabatic warming as it descends on the Argentine side of the Andes. During the LGM, the existence of ice sheets in Patagonia (e.g., Hulton et al. 2002; Lamy et al. 2004) acts to intensifying the orographic effect (Sime et al. 2013), since water vapor in the updraft airflow is much easier to condense and form precipitation within a colder environment. Thereby, rainfall increases (decreases) on the upwind side (leeside) of the mountains, leading to a dipole-like change of precipitation in this area (Cook and Vizy 2006). To summarize, local moisture-based proxies may not be reliable to represent the overall migration of SWW during the LGM. Indications from moisture proxies should be treated with caution.

Acknowledgments This work is primarily supported by NSF AGS-1249145. Jian Lu and L. Ruby Leung were partly supported by the Office of Science of the US Department of Energy as part of the Regional and Global Climate Modeling program. The Pacific Northwest National Laboratory is operated for DOE by Battelle Memorial Institute under contract DE-AC05-76RL01830.

References

Anderson RF, Ali S, Bradtmiller L, Fleisher MQ, Burckle LH (2009) Wind-driven upwelling in the Southern Ocean and the deglacial rise of atmospheric CO_2. Science 323:1443–1448

Bard E, Rickaby R (2009) Migration of the subtropical front as a modulator of glacial climate. Nature 460:380–393

Boos WR (2012) Thermodynamic scaling of the hydrological cycle of the Last Glacial Maximum. J Clim 25:992–1006

Braconnot P, Harrison SP, Kageyama M, Bartlein PJ, Masson-Delmotte V, Abe-Ouchi A, Otto-Bliesner BL, Zhao Y (2012) Evaluation of climate models using palaeoclimatic data. Nat Clim Change 2:417–424

Brady EC, Otto-Bliesner BL, Kay JE, Rosenbloom N (2013) Sensitivity to glacial forcing in the CCSM4. J Clim 26:1901–1925

Chavaillaz Y, Codron F, Kageyama M (2013) Southern westerlies in LGM and future (RCP4. 5) climates. Clim Past 9:517–524

Cook KH, Vizy EK (2006) Coupled model simulations of the West African monsoon system: twentieth-and twenty-first-century simulations. J Clim 19:3681–3703

Delmonte B, Petit JR, Maggi V (2002) Glacial to Holocene implications of the new 27000-year dust record from the EPICA Dome C (East Antarctica) ice core. Clim Dyn 18:647–660

Fraser CI, Nikula R, Spencer HG, Waters JM (2009) Kelp genes reveal effects of subantarctic sea ice during the Last Glacial Maximum. Proc Natl Acad Sci 106:3249–3253

Gersonde R et al (2003) Last glacial sea surface temperatures and sea-ice extent in the Southern Ocean (Atlantic-Indian sector): a multiproxy approach. Paleoceanography. doi:10.1029/2002PA000809

Gersonde R, Crosta X, Abelmann A, Armand L (2005) Sea-surface temperature and sea ice distribution of the Southern Ocean at the EPILOG Last Glacial Maximum—a circum-Antarctic view based on siliceous microfossil records. Quat Sci Rev 24:869–896

Held IM, Soden BJ (2006) Robust responses of the hydrological cycle to global warming. J Clim 19:5686–5699

Heusser L, Heusser CJ, Mix A, McManus J (2006a) Chilean and Southeast Pacific paleoclimate variations during the last glacial cycle: directly correlated pollen and d18O records from ODP Site 1234. Quat Sci Rev 25:3404–3415

Heusser L, Heusser CJ, Pisias N (2006b) Vegetation and climate dynamics of southern Chile during the past 50,000 years: results of ODP Site 1233 pollen analysis. Quat Sci Rev 25:474–485

Hulton NRJ, Purvesa RS, McCullocha RD, Sugdena DE, Bentleyb MJ (2002) The last glacial maximum and deglaciation in southern South America. Quat Sci Rev 21:233–241

Kalney E et al (1996) The NCEP/NCAR 40-year re-analysis project. Bull Am Meteorol Soc 77:437–471

Kim SJ, Flato GM, Boer GJ (2003) A coupled climate simulation of the Last Glacial Maximum, part 2: approach to equilibrium. Clim Dyn 20:635–661

Kitoh A, Murakami S, Kiode H (2001) A simulation of the last glacial maximum with a coupled atmosphere–ocean GCM. Geophys Res Lett 28:2221–2224

Kohfeld KE, Harrison SP (2001) DIRTMAP: the geologic record of dust. Earth Sci Rev 54:81–114

Kohfeld KE, Graham RM, de Boer AM, Sime LC, Wolff EW, Le Quéré C, Bopp L (2013) Southern Hemisphere westerly wind changes during the Last Glacial Maximum: paleo-data synthesis. Quat Sci Rev 68:76–95

Lamy F, Kaiser J, Ninnemann U, Hebbeln D, Arz HW, Stoner J (2004) Antarctic timing of surface water changes off Chile and Patagonian ice sheet response. Science 304:1959–1962

Mahowald NM et al (2006) Change in atmospheric mineral aerosols in response to climate: last glacial period pre-industrial, modern and doubled carbon dioxide climates. J Geophys Res Atmos. doi:10.1029/2005JD006653

Markgraf V (1989) Paleoclimates in central and South America since 18,000 BP based on pollen and lake-level records. Quat Sci Rev 8:1–24

Menviel L, Timmermann A, Mouchet A, Timm O (2008) Climate and marine carbon cycle response to changes in the strength of the Southern Hemispheric westerlies. Paleoceanography 23:PA4201

Nelson CS, Hendy IL, Neil HL, Hendy CH, Weaver PPE (2000) Last glacial jetting of cold waters through the Subtropical convergence zone in the Southwest Pacific off eastern New Zealand, and some geological implications. Palaeogeogr Palaeoclimatol Palaeoecol 156:103–121

Orsi AH, Whitworth T III, Nowlin WD Jr (1995) On the meridional extent and fronts of the Antarctic Circumpolar Current. Deep Sea Res I 42:641–673

Otto-Bliesner B, Brady EC, Clauzet G, Thomas R, Levis S, Kothavala Z (2006) Last glacial maximum and Holocene climate in CCSM3. J Clim 19:2526–2544

Paruelo JM, Beltran A, Jobbagy E, Sala OE, Golluscio RA (1998) The climate of Patagonia: general patterns and controls on biotic. Ecol Austral 8:85–101

Peeters FJC et al (2004) Vigorous exchange between the Indian and Atlantic Oceans at the end of the past five glacial periods. Nature 430:661–665

Petit JR et al (1999) Climate and atmospheric history of the past 420,000 years from the Vostok ice core, Antarctica. Nature 399:429–436

Prell WL et al (1980) Surface circulation of the Indian Ocean during the last glacial maximum, approximately 18,000 yr BP. Quat Res 14:309–336

Risien CM, Chelton DB (2008) A global climatology of surface wind and wind stress fields from eight years of QuikSCAT scatterometer data. J Phys Oceanogr 38:2379–2413

Rojas M (2013) Sensitivity of Southern Hemisphere circulation to LGM and 4xCO_2 climates. Geophys Res Lett 40:1–6

Rojas M, Moreno P, Kageyama M, Crucifix M, Hewitt C, Abe-Ouchi A, Ohgaito R, Brady EC, Hope P (2009) The southern westerlies during the last glacial maximum in PMIP2 simulations. Clim Dyn 32:525–548

Schäfer-Neth C, Paul A (2003) The Atlantic Ocean at the last glacial maximum: 1. objective mapping of the GLAMAP sea-surface conditions. In: Wefer G, Mulitza S, Ratmeyer V (eds) The South Atlantic in the Late Quaternary: material budget and current systems. Springer, Berlin, pp 531–548

Shin SI, Liu Z, Otto-Bliesner B, Brady EC, Kutzbach J, Harrison S (2003) A simulation of the Last Glacial Maximum climate using the NCAR-CCSM. Clim Dyn 20:127–151

Siani G, Michel E, De Pol-Holz R, DeVries T, Lamy F, Carel M, Isguder G, Dewilde F, Lourantou A (2013) Carbon isotope records reveal precise timing of enhanced Southern Ocean upwelling during the last deglaciation. Nat Commun 4. doi:10.1038/ncomms3758

Sime LC, Kohfeld KE, Le Quéré C, Wolff EW, de Boer AM, Graham RM, Bopp L (2013) Southern Hemisphere westerly wind changes during the Last Glacial Maximum: model-data comparison. Quat Sci Rev 64:104–120

Taylor KE, Stouffer RJ, Meehl GA (2012) An overview of CMIP5 and the experiment design. Bull Am Meteorol Soc 93:485–498

Toggweiler JR, Russell JL, Carson SR (2006) Midlatitude westerlies, atmospheric CO_2, and climate change during the ice ages. Paleoceanography 21:PA2005

Valdes PJ (2000) South American paleoclimate model simulations: how reliable are the models? J Quat Sci 15:357–368

Waelbroeck C et al (2009) Constraints on the magnitude and patterns of ocean cooling at the Last Glacial Maximum. Nat Geosci 2:127–132

Williams NJ, Harle KJ, Gale SJ, Heijnis H (2006) The vegetation history of the last glacial–interglacial cycle in eastern New South Wales, Australia. J Quat Sci 21:735–750

Wolff EW et al (2006) Southern Ocean sea-ice extent, productivity and iron flux over the past eight glacial cycles. Nature 440:491–496

Wyrwoll K-H, Dong B, Valdes P (2000) On the position of southern westerlies at the last glacial maximum: an outline of AGCM simulation results and evaluation of their implications. Quat Sci Rev 19:881–898

Yang J (2006) The seasonal variability of the Arctic Ocean Ekman transport and its role in the mixed layer heat and salt fluxes. J Clim 19:5366–5387